Chapter **5**

Interoperability of CWDM-routed reflective PONs

This chapter presents a complete multi-PON access network infrastructure by means of incorporating RSOAs to demonstrate wavelength independent ONUs and therefore network dynamicity. Critically the effect of RSOA application in coarse-WDM routing is described, followed by comprehensive optical and electrical characterisation of the RSOA, employed for both detection and modulation and revisiting of the network design parameters. Subsequently, the bidirectional transmission of a reflective WDM-PON over the coarse channel of the already described AWG has been modelled with the aim of demonstrating the potential of a single tunable laser in the OLT to dynamically address multiple colourless ONUs in the presence of PDW shift and worst case phase errors in the AWG.

5.1   Revised network architecture

The revised access network architecture is shown in Figure 5-1, utilising RSOA-based ONUs universally employed to demonstrate dynamic TDM and WDM-PONs, avoiding the necessity of wavelength-specific, local optical sources [1]. The multiple transceivers in the OLT, e.g. TL1 and TL2, are utilised to serve all reflective PONs by dynamically assigning downstream-transmission wavelengths to each ONU in tandem with CWs to be used by the RSOAs [2] for upstream transmission, allowing for cross-operational management of network load. However, the use of the RSOAs, with particular attention to injected signal power levels for upstream transmission and downstream detection in coarse-WDM routing will be shown to be affected by
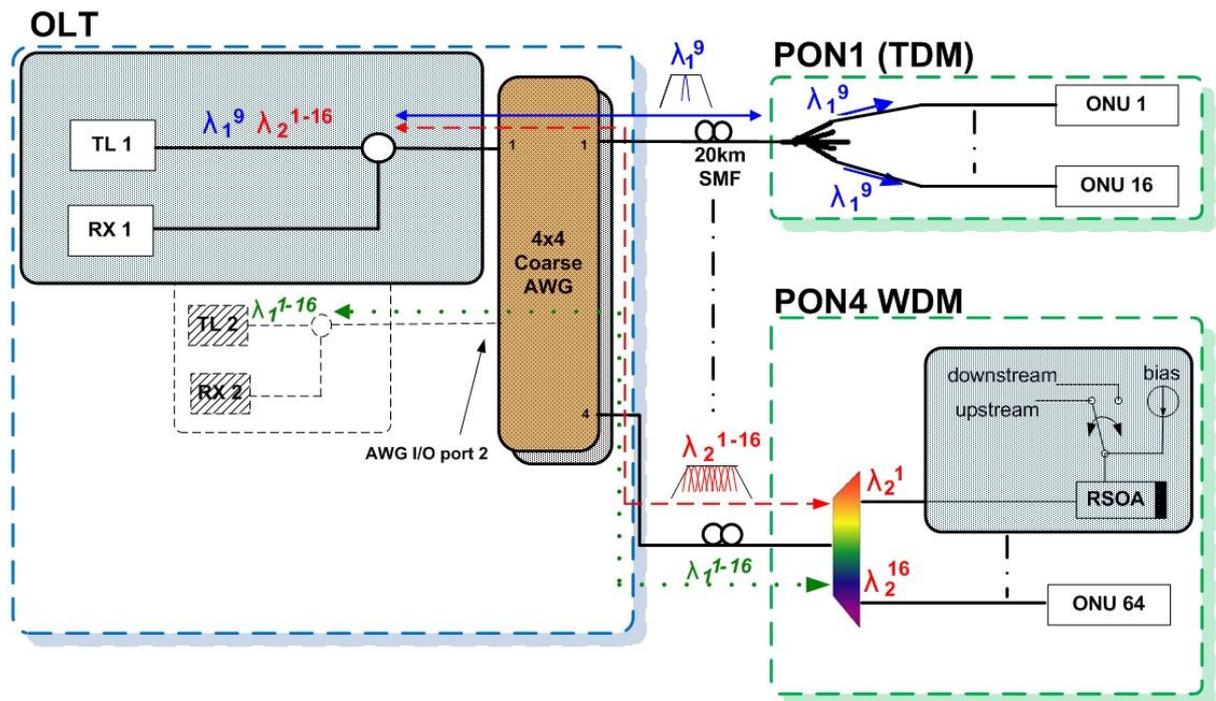
Figure 5-1 An interoperable access network based on CWDM-routed reflective PONs

the PDW of the AWG [3], which has been already demonstrated to degrade individual ONU routing performance of a PON. In addition, the OLT design is further investigated to provide CWs in addition to burst-data with sufficient power to overcome total network losses while avoiding the saturation of the RSOAs and variations in the reflected power among upstream wavelengths.

Displayed in Figure 5-1, downstream CWs, after reflected and modulated sequentially by the RSOAs will be routed upstream through exactly the same path utilised for their transmission in downstream. Consequently, all ONUs served by TL1 downstream will be terminated upstream to a single receiver, RX1, made possible due to the AWG's reciprocal nature [4] that allows the network to assign individual transceivers in the OLT to corresponding ONU clusters according to service categories, regardless ONUs physical location and wavelengths employed. Likewise, at the data-link layer, the OLT could assign each PON varying frame time-slots in order-of-demand to match bandwidth requirement, subsequently arranging bandwidth among

ONUs of each PON according to their bandwidth requirement, service level and overall capacity [5, 6]. Since the TL in the OLT is required to accommodate a wide tuning range of approximately 80 nm, corresponding to the spectra range occupied by all 4 physical PONs, commercially-available tunable lasers capable of covering such range with tuning time of 10 μs [7] are expected to provide sufficient performance to support data rates of up to 2.5 Gbit/s [8]. For higher data rates, a tuning capacity in the range of hundreds of nanoseconds will be required [8], however yet to become commercially-available for the required tuning range.

To establish optimal operation of the RSOA for both modulation and detection, the device input/output saturation power figures, ASE noise levels, gain bandwidth and electrical operating point characteristics have been recorded and will be explored in following sections. In that sense, due to power variations among downstream wavelengths caused by the coarse nature of the routing, while taking into account the saturating and gain figures of destination RSOAs, the network downstream performance and, as a result its upstream capabilities, due to reflectivity, will be shown to be influenced.

5.2   Reflective semiconductor optical amplifier operational characteristics

To determine the bias operating point of the modelled RSOA, functioning as a modulator or detector, the device reflected signal and ASE noise power level characteristics versus bias current, for diverse injected signal power levels, as generated in VPI are displayed in Figure 5-2. In order to produce such results, an unmodulated optical signal at 1550 nm, equivalent to the RSOA central gain curve, was applied at the device input and the corresponding reflected power levels were recorded with an optical power meter, connected via a 50 GHz-wide BPF to reduce the ASE noise level. As becomes evident from the figure with respect to bias currents, the reflected power level begins to saturate at output power levels in the range of -3 dBm to +1 dBm, indicated by the vertical line.   It can be further observed that the reflected signal and ASE noise power levels increase with bias current, however, as opposed to a practical RSOA performance, do not fully saturate in higher bias currents since thermal effects are not taken into account in the standard VPI RSOA module [9]. Finally, as displayed in the inset for the figure, the ASE noise power decreases by increasing the injected signal power level due to saturation [2], resulting in optical signal to noise ratios (OSNRs) in the range of 17 dB to 24 dB, as expected from the performance characteristics of a practical RSOA [2].
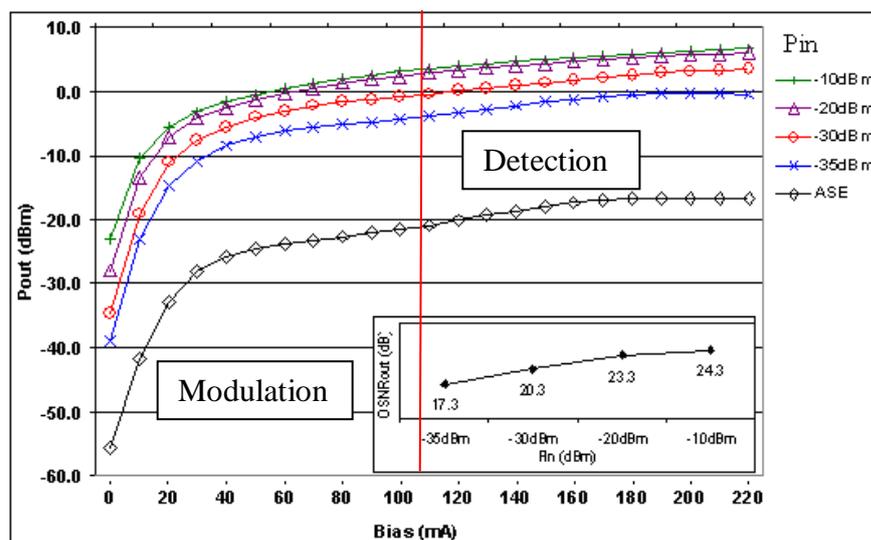

Figure 5-2 RSOA reflected signal and ASE noise power versus bias current

Figure 5-3 shows the RSOA gain characteristics versus injected signal power for different bias currents used for detection and modulation, when the RSOA input is injected with an optical carrier at 1550 nm. As becomes apparent from the figure, the device gain saturates, i.e. typically drops by 3 dB, at injected signal power level of -28 dBm, allowing for a maximum gain in the range of 25 dB to 29 dB corresponding to bias currents from 50 mA to 110 mA. Consequently, a maximum reflected power between -3 dBm to +1 dBm can be achieved, sufficiently to provide upstream power for all ONUs to overcome subsequent network losses. These gain figures are higher than those of a practical device, as analysed in details in chapter 7, due to the limitation of the RSOA module to include the trade-off between optical gain and electrical bandwidth. In that sense, the RSOA provides similar gain for both optical carrier amplification and data modulation, though, under no circumstances the use of the RSOA in the simulations changed the network upstream transmission performance, when compared to the experimental results in chapter 7. Nevertheless, this is believed to be rectified by establishing a private communication with VPI.
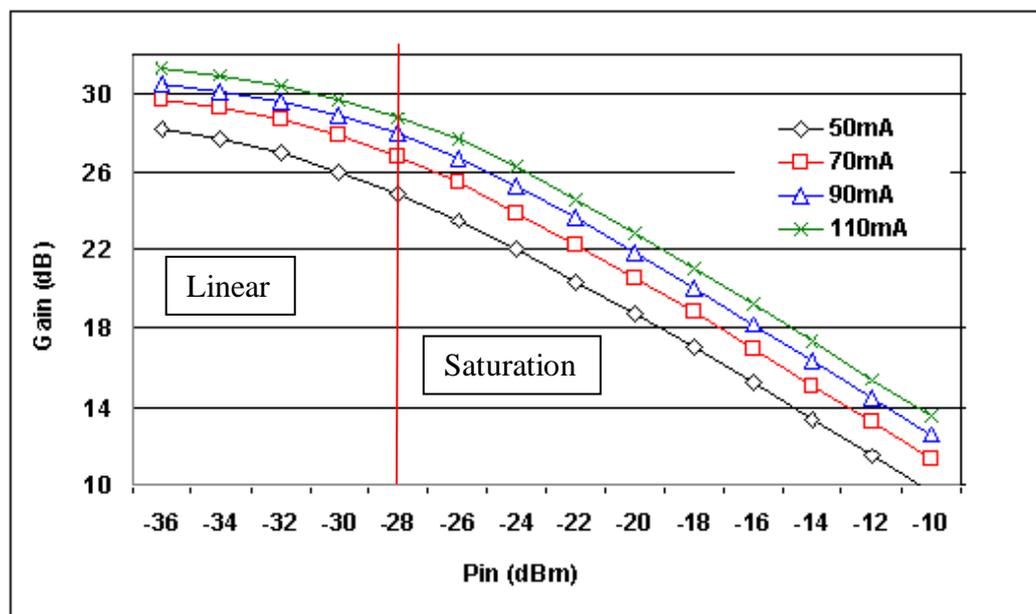

Figure 5-3 RSOA gain versus injected signal power

From the behaviour recorded in Figure 5-2, the RSOA operation can be divided into linear and saturation regimes for which, modulation is better performed at the former whilst detection in the later [2].

5.2.1 Modulation

As suggested by the linear portion of the traces in Figure 5-2, low-level bias currents demonstrate sharper slope, as opposed to higher bias levels, consequently being more appropriate for modulation where high ER and low ASE noise are required. To achieve optimal modulation in the RSOA, the bias current modulation levels were set just above the threshold level of 8.7 mA for logic "0" and 108 mA for logic "1" to provide maximum optical power, while avoiding to electrically overdrive the RSOA, at an ER of 12 dB following a typical figure of a practical RSOA [2]. This is verified by Figure 5-4 for the transmitted eye diagram at the RSOA optical reflected output, representing a modulated 1550 nm optical carrier injected at -28 dBm. An open eye diagram can be observed due to a moderate amount of ASE noise superimposed at logic "1" and less significant ASE noise power around the "0's". This can be further analysed from the modulation regime in Figure 5-2, for which a power difference of 20 dB can be observed between 0 dBm optical power for logic "1" and -20 dBm noise floor power at corresponding bias current. Comparable ASE noise levels cannot be met for the "0's" with noise power of around -42 dBm, allowing for similar power difference of 20 dB due to -22 dBm optical power for logic "0".
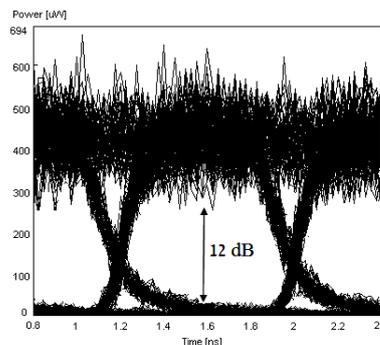

Figure 5-4 Extinction ratio of RSOA transmitted signal

5.2.2 Detection

The detection process includes sensing of the differences in voltage produced at the bias electrode of the RSOA [2, 10]. As illustrated in Figure 5-5, a change of injected signal power level at the device optical input will lead to inversely proportional variations in carrier density taking place inside the device cavity [11]. Subsequently, the variations in voltage at the bias electrode are directly proportional to those variations in carrier density within the device cavity [2], given by,

$$\Delta V = \eta \frac{kT}{q} \ln\left(\frac{N_i + \Delta N}{N_i} \right)$$

(5.1)

where η is the junction ideality factor, typically 2 [12], representing a measure of how closely the amplifier follows an ideal light-current (L-I) curve with a factor of 1. k is Boltzmann's constant $1.3806503 \times 10^{-23}$ J/K, T the junction absolute temperature 300° K, q the electronics charge 1.602×10^{-19} C, ΔN (m^{-3}) corresponds to the variation in carrier density, and Ni (m^{-3}) is the intrinsic carrier density in the active region i.e. when no light is injected [12].

To allow efficient detection in the saturation regime where the OSNR is higher, a bias current of 108 mA was utilised, corresponding to logic level "1" as described in section 5.2.
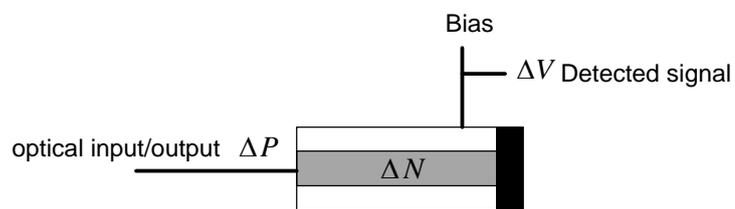

Figure 5-5 RSOA block diagram

5.2.3 Gain and amplified spontaneous emission noise

Figure 5-6 shows the ASE noise spectra for various bias currents measured at the device optical reflected output when no light is injected to its optical input. The two vertical lines in the figure represent approximately 30 nm ASE noise spectral width at 3 dB, reflecting directly on the available gain bandwidth centred around 1550 nm of the device. As expected, the noise power level increases with bias current, however demonstrates lesser power difference at bias currents of around 110 mA, consequently confirming the gain saturation observed previously in section 5.2. In order to investigate the effect of ASE noise and gain on fully-populated WDM ONUs, at least 20 nm gain bandwidth needs to be accounted in the simulation to include not only the 7 nm spectrum occupied by the ONUs but also the noise superimposed over of the entire AWG passband outside the 7 nm, which is equivalent to the channel spacing of the AWG. Nevertheless, to allow in practice the amplification of all four coarse passbands of the AWG, as it is discussed in details in chapter 8, a wider gain bandwidth is required.
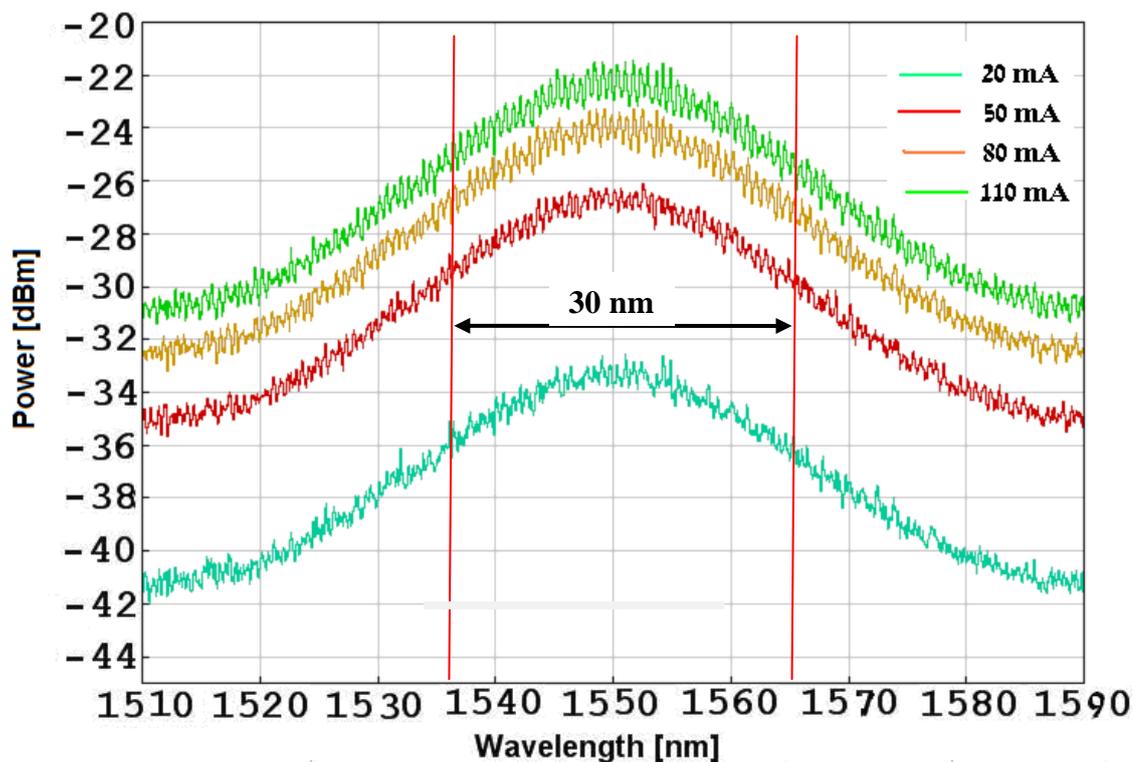
Figure 5-6 RSOA ASE noise spectra

5.2.4 Electrical bandwidth response

Commercially-available RSOA devices utilise relatively low electrical bandwidth, e.g. 1.2 GHz [13], consequently limiting the modulation and detection speeds. To assess the electrical bandwidth of the modelled RSOA, Figure 5-7 shows the measured electrical frequency response when a modulated optical signal at 1550 nm and power level of -28 dBm, representing the highest optical power to avoid saturation, was injected into the model along with a power meter, used to measure the detected signal power level. It can be observed that although the frequency response is not entirely flat in the lower region, the electrical bandwidth is approximately 900 MHz. To accommodate upstream and downstream signals corresponding to the available bandwidth, the data rate for detection and modulation was limited to 1.25 Gbit/s, which is the highest data rate that can be achieved using NRZ encoding in on-off keying modulation [14]. Only recently, a major photonics vendor has established upstream transmission at 2.5 Gbit/s [15], which is expected to accommodate the data rates originally proposed for the multi-PON architecture in future designs.
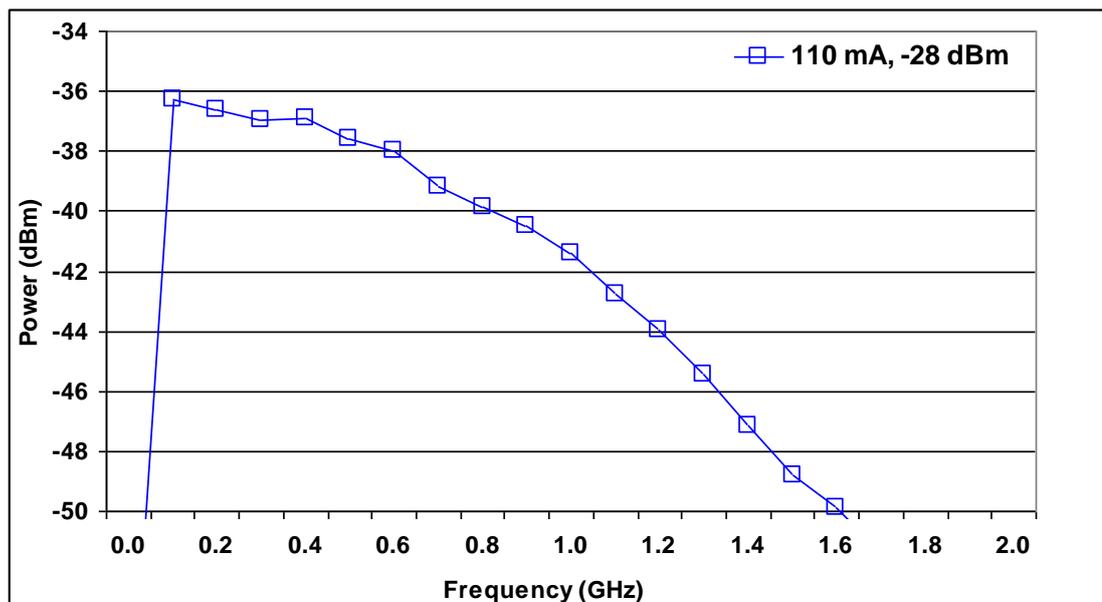

Figure 5-7 RSOA electrical bandwidth response

5.3   Reflective ONU design

The physical layer ONU modelling comprising standard network elements and the originally implemented RSOA device were developed using the VPI simulation platform.   Particular emphasis was paid in biasing the RSOA and defining physical properties for downstream signal detection.   This can be achieved in VPI only by converting the carrier density of the device to detected downstream voltage by means of observing the model's contact output, as previously described in equation 5.1.   In contrast, practical devices do not display a contact output since the detected signal is taken from the bias contact.   Subsequently, a novel optimisation technique to reduce simulation time while displaying practical figures of broadband ASE noise is established and employed in the simulations.

5.3.1 Modelling characteristics

The RSOA and extension ONU models are shown in Figure 5-8.   Initially, a standard VPI PRBS module is employed in conjunction with a laser driver for biasing the RSOA via its bias input electrode and modulating the downstream CWs for upstream transmission.   Following the optical path downstream, an optical attenuator is initially used to obtain downstream BER performance characteristics.   Subsequently, the detected signal is received via the designed RSOA model bias output electrode where it is applied at a BER and scope modules, employed also to obtain BER performance characteristics and display eye diagrams respectively.   In addition, an optical power meter, applied at the RSOA optical output port is also connected to help establishing the network BER performance.
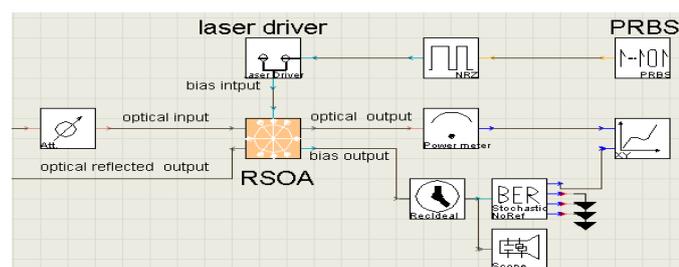
Figure 5-8 RSOA-based ONU modelling

In upstream, each injected CW is amplified by the RSOA, subsequently modulated via the bias input electrode and reflected back via the optical reflected output port of the RSOA.

VPI Table 5-1 includes the modelling parameters of the PRBS employed for both upstream and downstream transmissions. In upstream, a 1.25 Gbit/s, 2^7-1 long PRBS was utilised to comply with the limited RSOA electrical frequency response of 900 MHz as explained in previous sections. The PRBS bit rate parameter is determined in the global simulation parameter "BitRateDefault". In downstream, a sequence of "1's" was constantly supplied to the laser driver shown in Figure 5-8, to provide 108 mA at the bias input of the RSOA for detection.

Table 5-1 PRBS modelling parameters

f	BitRate	BitRateDefault	bit/s
i	PreSpaces	0	
i	PostSpaces	0	
	PRBS_Type	PRBS_N/One	
f	MarkProbability	0.5	
i	PRBS_Order	7	
i	MarkNumber	7	

The laser driver parameters are shown in Table 5-2. The injected current modulation levels are determined according to the logical-level $\times$ DriveAmplitude + Bias, i.e. to convert a logic "0" and "1" to a Bias and Bias plus DriveAmplitude currents, corresponding to 8.7 mA and 108 mA, providing reflected signal power for each CW at approximately 0 dBm and ER of 12 dB for the central wavelength at λ_2^9=1550.12 nm as previously established.

Table 5-2 Laser driver modelling parameters

f	DriveAmplitude	0.100	A, V
f	Bias	0.0087	A, V

5.3.2 RSOA module in detection and modulation

To deepen into the RSOA model, Figure 5-9 displays a standard VPI semiconductor optical amplifier (SOA) module that is configured as an RSOA device, comprising optical I/O ports, a bias input electrode and a contact output electrode particularly employed for the measurement of carrier density in the device cavity. To convert the carrier density variation to detectable voltage, electrical samples at the contact output are initially converted to native VPI samples to be mathematically manipulated by the semiconductor junction parameters in the RSOA. In that direction, the native samples are multiplied by a constant, corresponding to a measured intrinsic carrier density *Ni* of 0.925×10^{-24} m^{-3} and subsequently the logarithm of their product is further mathematically processed to account for the additional semiconductor junction parameters, as shown in equation 5.1. Finally, the samples are converted back to electrical form, coupled to a LPF, employed for limiting the electrical noise, and via an electrical inverter turn inversely proportional to the input optical signal variations. In the case of modulation, the bias input port is used for modulating the injected optical signal that is subsequently reflected via the optical reflected output port.
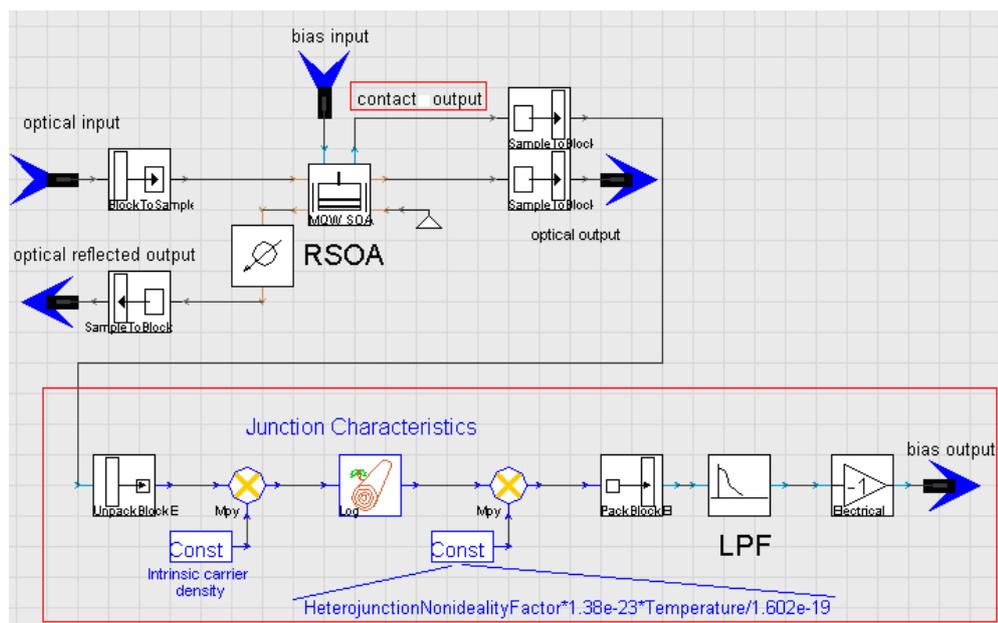

Figure 5-9 RSOA modelling in details

The physical parameters of the SOA device are displayed in VPI Table 5-3. Particular attention was given to the amount of reflection of the device right facet, ASE noise spectral characteristics and wavelength operation. The centre wavelength operation was determined by a global parameter "SampleModeCentreFrequency", set to 1550 nm, representing a commercially-available RSOA device [16]. The nominal wavelength parameter shown in the table to represent the wavelength used for photon energy calculation was set to the centre wavelength of the RSOA. A left facet reflectivity of 10^{-7} was utilised to allow the reflected signal exit the device cavity avoiding the formation of unwanted reflections causing oscillations. Finally, to allow approximately 30 nm-wide gain bandwidth, the parameters "SpontaneousEmissionSpectralWidth" and "GainCoefficientSpectralWidth" were set to 4.7 THz and 2.1×4.7 THz respectively. The gain coefficient spectral width was set higher than the spontaneous emission spectral width to match the VPI design characteristics [12].

Table 5-3 RSOA modelling physical parameters

f	NominalWavelength	1550e-9	m
f	LaserChipLength	505.65e-06	m
f	ActiveRegionWidth	1.2e-06	m
f	ActiveRegionThickness	0.056e-06	m
f	OneSide_SCH_RegionThickness	0.059e-06*5	m
f	MQWsConfinementFactor	0.045	
f	SCH_ConfinementFactor	0.4	
f	GroupEffectiveIndex	3.7	
f	OpticalCouplingEfficiency	0.5	
f	FixedInternalLoss	1000.0	1/m
f	CarrierDependentInternalLossCoefficient	0.0	m^2
f	MQW_MaterialLinewidthEnhancementFactor	3.0	
f	MQW_DifferentialRefractiveIndex	-1.11e-26	m^3
f	SCH_DifferentialRefractiveIndex	-1.50e-26/5	m^3
f	ChirpReferenceCarrierDensity	2.0e+24	1/m^3
f	GainPeakFrequency	0.0	Hz
f	GainPeakFreqCarrierDependence	0.0	Hz m^3
f	GainCoefficientSpectralWidth	2.1*4.7e12	Hz
f	GainCoeffSpectralWidthCarrierDependence	0.0	Hz m^3
f	PopulationInversionParameter	1e-4	
f	SpontaneousEmissionPeakFrequency	0.0	Hz
f	SpontaneousEmissionFreqCarrierDependence	0.0	Hz m^3
f	SpontaneousEmissionSpectralWidth	4.7e+12	Hz
f	SpontaneousSpectralWidthCarrierDependence	0.0	Hz m^3
f	InitialCarrierDensity	2.0e+24	1/m^3

5.3.3 Time-optimisation in the presence of broadband ASE

In an amplified system the bandwidth of the modulated data signal is much narrower than the bandwidth of the ASE noise propagating through the network. Though, it is significant to simulate the entire noise bandwidth since it will lead to post-detection electrical noise that is expected to degrade the BER performance. ASE noise typically spreads over several THz, i.e. tens of nano-meters, which if converted to transmission VPI samples, results to excessive simulation time which in many cases has caused the simulation to halt [17]. To avoid this, a more sophisticated approach was utilised, allowing separation of the ASE noise and optical data signals spectrum in order to represent the sampled noise by noise bins (NB) [17]. Noise bins assume the noise spectral density is constant over a block of data and as a result it can be represented by the average spectral density in two polarisations. Furthermore, NB may adapt in bandwidth statistically to provide efficient spectral resolution [17] as shown in Figure 5-10.
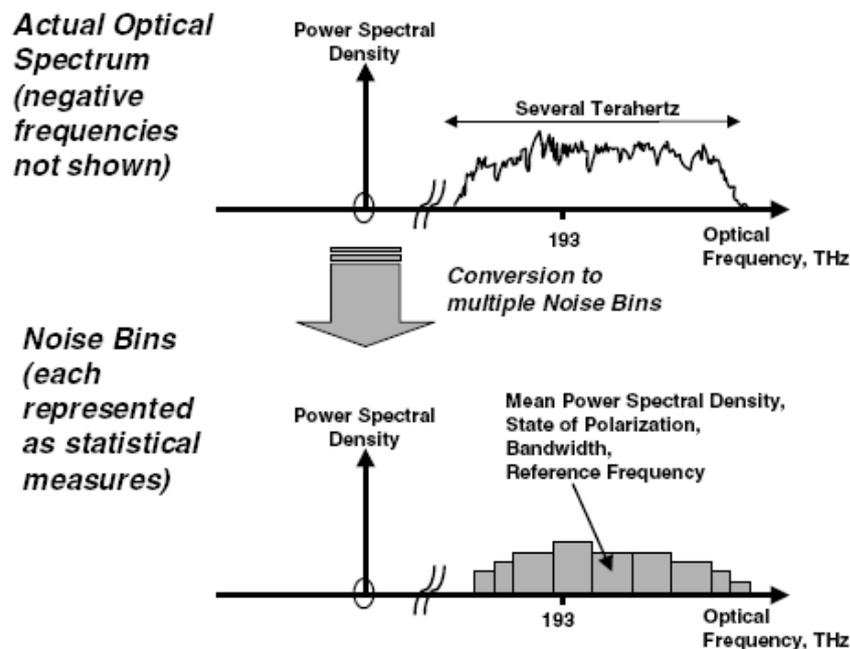

Figure 5-10 Representation of wide-band noise with noise bins [17]

In the simulation, a bandwidth of 2450 GHz corresponding to a standard 20 nm channel spacing of the coarse AWG was utilised. Since the standard VPI SOA model [18], and as a result the newly devised RSOA described so far does not support the use of NB, an innovative simulation approach shown in Figure 5-11 was devised to convert the sampled ASE noise into NB. As shown in the figure, the sampled ASE noise and modulated data signals are distributed into two independent arms without any modification in power or spectra. Subsequently, the modulated data signal and ASE noise spectra in each arm are separated by means of a 20 GHz, 3 dB bandwidth BPF in the bottom arm, centred on the wavelength of the optical data and noise signals to only allow transmission of the modulated signal spectrum, and a notch filter in the upper arm with similar bandwidth and wavelength characteristics to block the modulated data signal, allowing only the sampled noise through. Finally, the sampled ASE noise is converted to NB in the signal-converter module with a measured optimum resolution of 80 GHz to allow for the right balance between simulation time and power level accuracy, and subsequently re-coupled with the modulated data signals using an ideal combiner.
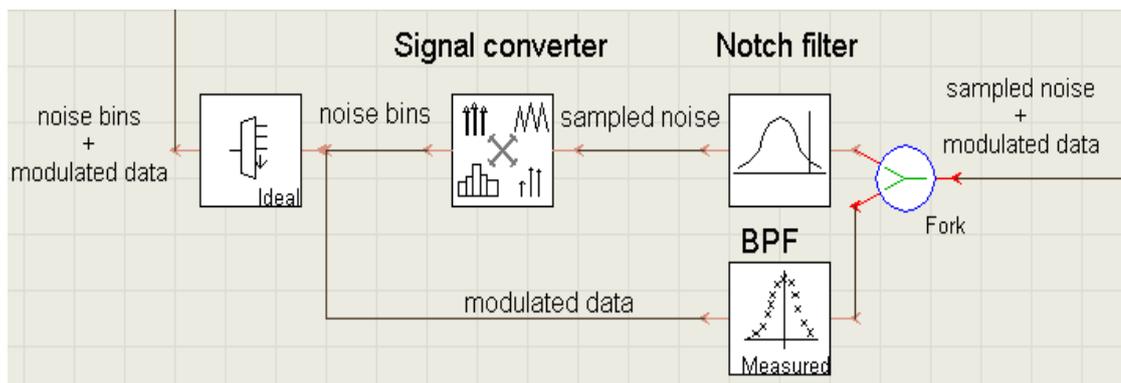

Figure 5-11 Sampled noise to noise bins conversion model

To evaluate the model, the spectrum of both the sampled upstream transmission and corresponding data and NB for the central wavelength at $\lambda_2{}^9$=1550.12 nm were compared visually and verified with power measurements using an optical power meter. Subsequently, Figures 5-12(a) and (b) represent the upstream transmission spectra before and after conversion respectively. In that sense, the ASE noise, shown in Figure 5-12(a), exhibits fairly constant power spectral density with no more than 1.2 dB variations across the entire spectrum. When compared to the spectrum shown in Figure 5-12(b), a good agreement is met in terms of power spectral density with measured difference in optical power of less than 0.5 dB between the two transmissions, with particular attention to the data element that remains intact.
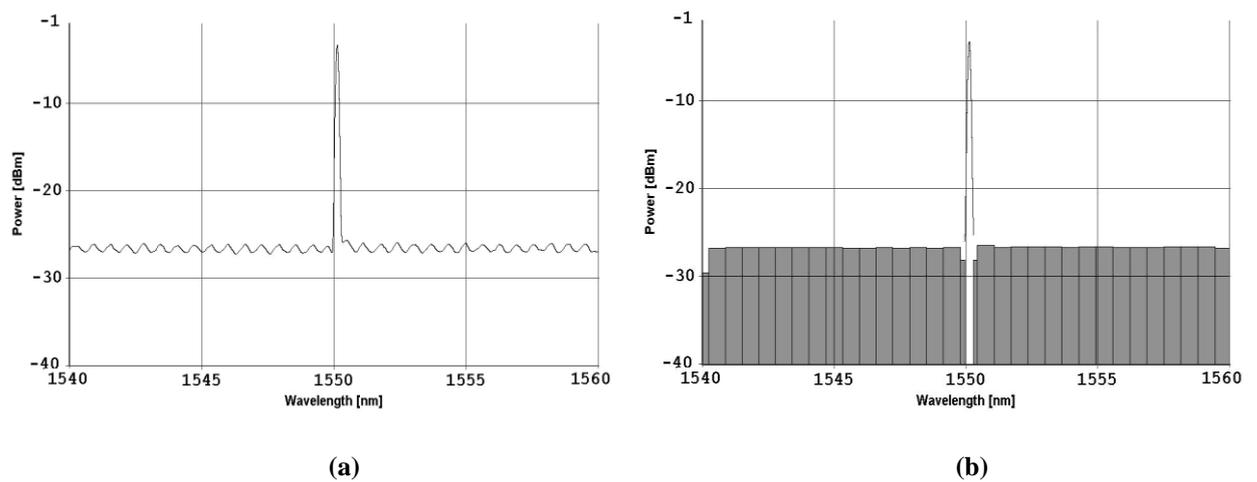

(a)   (b)

Figure 5-12 Representation of RSOA transmission spectrum (a) samples (b) noise bins

As previously mentioned, the spectral width of individual NB may be, in some cases, critical to statistically represent the noise with minimum variations in power when compared to the original samples. This is particularly true in the scenario when subsequent network elements passband response, such as for the distribution point demultiplexer and coarse AWG, are capable of reshaping the ASE spectra from its constant power spectral density, as shown previously in Figure 5-12(a), to a form demonstrated in Figure 5-13(a). Figure 5-13(a) represents the spectrum of the upstream transmission prior detection in the OLT while the conversion model is inactive. The two peaks both sides of the central wavelength are the consequence of the multiple FSRs of the AWG. Also, the shape of the ASE noise located between the peaks is the result of the AWG phase errors.

In order to find the optimum NB resolution to allow comparable ASE noise spectral density, the conversion model was set active and a range of NB resolution values have been sequentially employed while the noise bins representation of the upstream transmission was visually observed, accompanied by optical power measurements. In that direction, an optimum 80 GHz bandwidth of all individual NB was ultimately utilised providing a good agreement met, as shown in Figure 5-13(b), with measured difference in power of less than 0.5 dB.
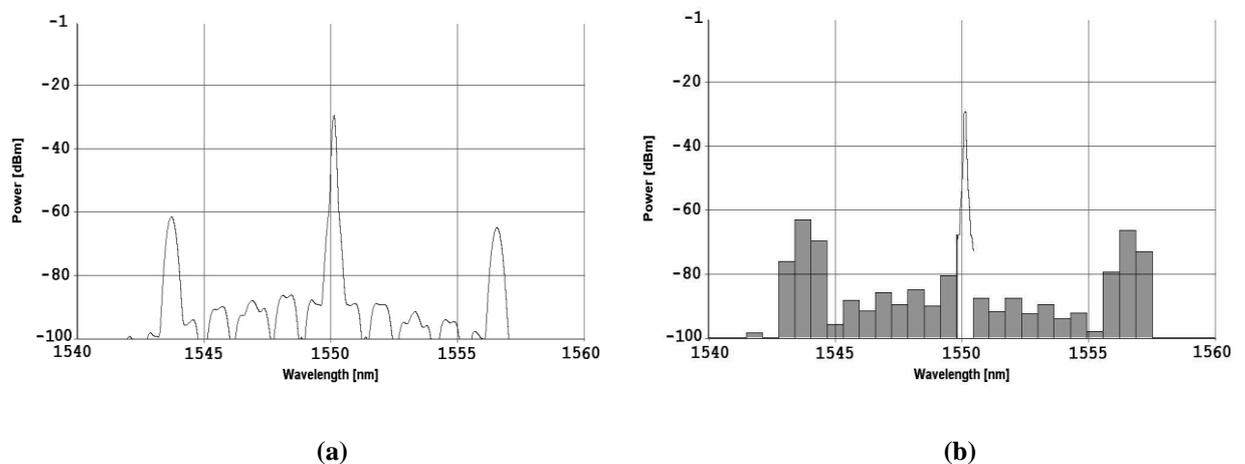

(a)   (b)

Figure 5-13 Representation of upstream transmission prior detection in the OLT (a) samples (b) noise bins

5.4   WDM-PON transmission performance

A physical layer simulation testbed, shown in Figure 5-14, was devised to model the network potential to route bidirectionally multiple RSOA-based WDM ONUs (see appendix C.2 for VPI schematic). In preference to chapter 4, the ONUs have been completely rectified in the sense that all their elements have been replaced by a single RSOA accompanied with electrical circuit utilised for biasing. To support this, the OLT transmission power level has been readjusted to provide downstream CWs with sufficient power for upstream transmission by the RSOAs, while avoiding their saturation, and by taking into account its direct relation to Rayleigh backscattering propagating in the upstream direction.

Significantly, to investigate the influence of the Gaussian response and passband shifting in the power distribution and routing performance of individual incident and reflected wavelengths, a fully-populated WDM-PON (PON4) with 16 ONUs was simulated.
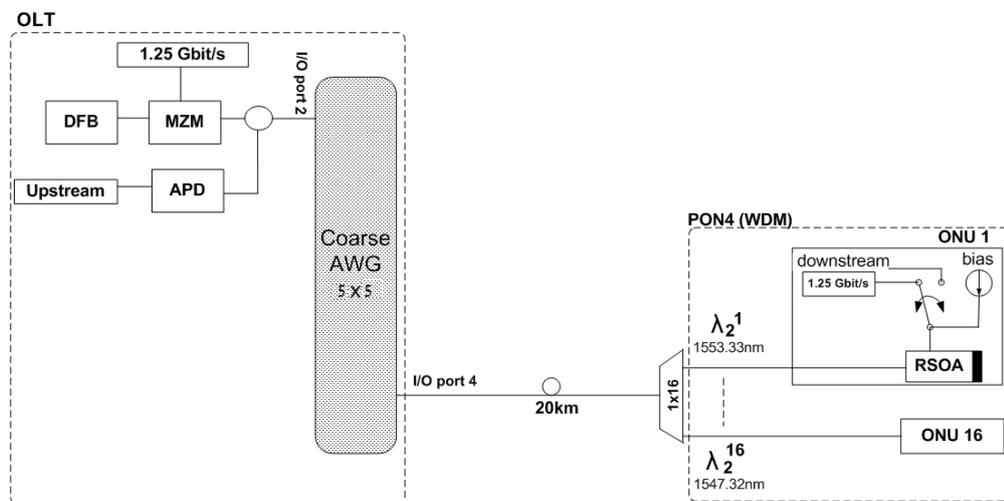

Figure 5-14 Simulation testbed utilising RSOA-based ONUs

As shown in Figure 5-14, a MZM was used in the OLT to externally modulate a DFB laser at -9 dBm to supply CWs in downstream with sufficient power while avoiding to saturate the RSOAs in destination ONUs with a 1.25 Gbit/s, 2^7-1 long PRBS employed at the modulator's

RF input as already justified.   Modulated, 0.4 nm-spaced wavelengths, spread across λ_2^1=1553.33 nm and λ_2^{16}=1547.32 nm representing network ONUs were applied initially to a circulator to allow bidirectional transmission and via the AWG downstream I/O port 2 routed through the AWG coarse channel λ_2=1550 nm to output I/O port 4 and coupled to 20 km of SSMF. At the distribution point, a 1×16 demultiplexer communicated the optical signals to the designated ONUs. Once inside each network unit, downstream wavelengths were detected by means of voltage variation at the RSOA bias output electrode explained in detail in previous sections.

In upstream, each injected CW at maximum power of -28 dBm, to avoid saturation of the RSOA, was amplified and subsequently reflected back from the device at approximately 0 dBm to be modulated in turn by another random sequence with the same length and data rate to demonstrate upstream transmission, at an ER of 12 dB, through exactly the same path followed downstream. As a result, all ONUs from PON4 were routed upstream collectively to a common AWG output port 2 by means of the nominated coarse passband denoted by λ_2 and terminated to a single OLT receiver, RX1.

An approximate, 1 dB polarisation-dependent gain (PDG) typical of polarisation-independent RSOAs [16] was not accounted for in the model to reduce RSOA modelling complexity by means of a combined modulating/detecting device and the excessive simulation time.

5.4.1 Network power budgeting

The network is designed in terms of power budgeting with respect to individual components losses throughout the optical path and the gain of RSOAs in the ONUs and very importantly, as repeatedly mentioned avoiding to saturate the RSOAs in destination ONUs to allow error-free transmission of all wavelengths of the WDM-PON. Analysis of power budget measurements for the most severely degraded ONU at maximum PDW shift is summarised in Table 5-4.

Table 5-4 Network power budget

Parameter	Value	
DFB launched power	-9 dBm	
MZM insertion loss	5 dB	
Optical circulator	1 dB	
Coarse AWG loss @ longest wavelength	10.5 dB	
20 km SSMF loss	4 dB	
Distribution point losses	5.5 dB	
RSOA gain	reflected	incident
	30 dB	16 dB
RSOA sensitivity @ 10^{-9} BER		-17 dBm
RSOA reflected power @ longest wavelength	-5 dBm	
Upstream network losses	21 dB	
APD sensitivity @ 10^{-9} BER	-27.75 dBm	

According to Table 5-4 the highest downstream link loss ranging up to 26 dB between the DFB laser in the OLT and the RSOA in the ONU was recorded at the longest wavelength λ_2^1 = 1553.33 nm of the AWG transmission passband. This includes the typical losses of a MZM, distribution point multiplexer, 20 km SSMF and optical circulator, in addition to wavelength-specific coarse AWG losses depending on its Gaussian response and PDL.

In upstream, a 21 dB maximum link loss was displayed between the RSOA in the ONU and the APD in the OLT once again for the longest wavelengths of all AWG passbands.

5.4.2 Bit-error-rate analysis

To evaluate the downstream and upstream network transmission capabilities, BER responses are drawn in Figure 5-15(a) for the least and most severely degraded ONUs of WDM-PON4. Results confirm error-free transmission with measured BER of 10^{-9} achieved by all upstream ONUs at the expense of a maximum 2.5 dB power penalty between λ_2^9 and λ_2^1, reflecting closely the extra acquired PDL.

Similar error performance was recorded in downstream at increased received power due to the limited sensitivity figure of the RSOA. The curve displayed in Figure 5-15(a) for downstream transmission corresponds to wavelength λ_2^2, representing the last detectable wavelength at an error rate of 10^{-9}. This is true since at the worst case scenario PDW of 1.8 nm, λ_2^1 displayed insufficient power to maintain error-free performance with no compensation applied at the risk of driving the RSOA in saturation. Further investigations of the highest possible PDW attainable downstream to allow all wavelengths to be transmitted, produced a figure of 0.8 nm. This is confirmed in Figure 5-15(b), where error rate of 10^{-9} was achieved by the most severely degraded wavelength λ_2^1 downstream. In upstream, similar error performance was recorded for all wavelengths with reduced power penalty of 1.3 dB between λ_2^9 and λ_2^1 reflecting closely the extra acquired PDL of 1.3 dB measured for λ_2^1.
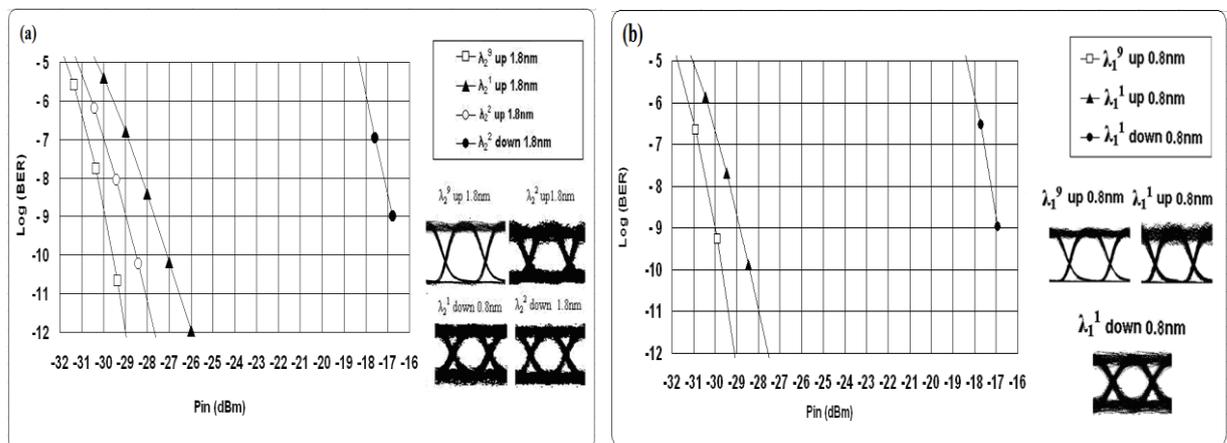

Figure 5-15 Measured BER for upstream and downstream transmission at (a) 0.8 nm (b) 1.8 nm

5.5 Summary

This chapter presented full implementation of the CWDM network architecture of chapter 4 complemented by the employment of RSOAs in ONUs to add reflectivity in TDM and WDM-PONs and therefore colourless, universal ONU customer premises equipment (CPE). Consequently, the OLT design presented in chapter 4 was modified to provide CWs in addition to burst-data downstream for upstream transmission, while the laser and detector in each ONU were replaced by a single RSOA utilised for both modulation and detection. The optical and electrical characteristics of the RSOA model were optimised, while a novel modelling technique was proposed to increase the speed of simulation in the presence of broadband ASE noise.

The ONU reflectivity supplements the inherited network dynamicity in the sense of assigning bandwidth to multiple PONs through a single TL, allowing the OLT choose which PON to serve for longer time according to bandwidth requirement, and increased scalability in providing multiple wavelengths in existing WDM ONUs and integrating additional TDM ONUs to increase network penetration. This is achieved by connecting extra transceivers at appropriate AWG ports of a single OLT. Employing the same wavelengths for bidirectional transmission in each RSOA-based ONU, adds extra dynamism since the OLT can reassign time-slots used for burst data and CWs to grant upstream and downstream data transfer on demand.

Network modelling results using a single AWG and a single TL in the OLT to address multiple colourless RSOA-based ONUs of a fully populated WDM-PON have confirmed error-free routing of 16, 0.4 nm-spaced wavelengths over the AWG 1550 nm, 7 nm-wide Gaussian channel, in the presence of 0.8 nm PDW shifting and 270° worst case phase errors. Further

investigations have confirmed that more than 93% of the ONUs sustain 10^{-9} error rates for extended worst case PDW of 1.8 nm.   5-23

5.6   References

[1]   Y. Shachaf, P. Kourtessis, and J. M. Senior, "An interoperable access network based on CWDM-routed PONs," presented at 33rd European Conference and Exhibition on Optical Communication (ECOC), Berlin, Germany, 2007.

[2]   J. Prat, C. Arellano, V. Polo, and C. Bock, "Optical Network Unit Based on a Bidirectional Reflective Semiconductor Optical amplifier for Fiber-to-the-Home Networks," *IEEE Photonics Technology Letters*, vol. 17, pp. 250-253, 2005.

[3]   J. Jiang, C. L. Callender, C. Blanchetière, J. P. Noad, S. Chen, J. Ballato, and J. Dennis W. Smith, "Arrayed Waveguide Gratings Based on Perfluorocyclobutane Polymers for CWDM Applications," *IEEE Photonics Technology Letters*, vol. 18, pp. 370-372, 2006.

[4]   I. Tsalamanis, E. Rochat, and S. D. Walker, "Experimental demonstration of cascaded AWG access network featuring bi-directional transmission and polarization multiplexing," *OSA Optics Express*, vol. 12, pp. 764-769, 2004.

[5]   C.-H. Chang, P. Kourtessis, and J. M. Senior, "GPON service level agreement based dynamic bandwidth assignment protocol," *Journal of Electronics Letters*, vol. 42, pp. 1173-1174, 2006.

[6]   C.-H. Chang, P. Kourtessis, and J. M. Senior, "Dynamic Bandwidth assignment for Multi-service access in GPON," presented at 12th European Conference on Networks and Optical Communications (NOC), Stockholm, Sweden, 2007.

[7]   J. Buus, J. Buus, and E. J. Murphy, "Tunable lasers in optical networks," *IEEE/OSA Journal of Lightwave Technology*, vol. 24, pp. 5-11, 2006.

[8]   C. Bock, J. Prat, and S. D. Walker, "Hybrid WDM/TDM PON using the AWG FSR and featuring centralized light generation and dynamic bandwidth allocation," *IEEE/OSA Journal of Lightwave Technology*, vol. 23, pp. 3981-3988, 2005.

[9]   V. Volkov, "Private communication." Berlin, Germany: Virtual Photonics Inc, 2005.

[10]   J. O'Carroll and M. J. Connelly, "Gate Array Signalling Information Detection using a Semiconductor Optical Amplifier," presented at First Joint IEI/IEE Symposium on Telecommunications Systems Research, Clyde Road, Dublin, 2001.

[11]   T. Rampone, H.-W. Li, and A. Sharaiha, "Semiconductor Optical Amplifier Used as an In-Line Detector with the Signal DC-Component Conservation," *IEEE/OSA Journal of Lightwave Technology*, vol. 16, pp. 1295-13-1, 1998.

[12]   "Active Photonics User's Manual," VPIcomponentMaker, VPIphotonics Inc., 2006.

[13]   CIP-Photonics,

        "http://www.ciphotonics.com/PDFs%20May08/SOA_RL_OEC_1550_J.pdf," 2008.

[14]   K. Inoue, "Influence of fiber four-wave mixing in multichannel return-to-zero (RZ) signal transmissions," *IEEE Photonics Technology Letters*, vol. 8, pp. 293-295, 1996.

[15]   A. Borghesani, I. Lealman, D. Smith, A. Poustie, and R. Wyatt, "High Temperature, Colourless Operation of a Reflective Semiconductor Optical Amplifier for 2.5Gbit/s upstream transmission in a WDM-PON (Invited)," presented at 33rd European Conference and Exhibition on Optical Communication (ECOC), Berlin, Germany, 2007.

[16]   CIP-Photonics, "http://www.ciphotonics.com/cip_semiconductor_2.htm," 2006.

[17]   "WDM User's Manual," VPItransmissionMaker, VPIphotonics Inc., 2006.

[18]   "http://www.vpiphotonics.com/," VPIphotonics Inc., 2007.